*J. Fluid Mech.* (2000), *vol.* 416, *pp.* 151–172. Printed in the United Kingdom



# Experimental characterization of viscoelastic effects on two- and three-dimensional shear instabilities

By OLIVIER CADOT[1] AND SATISH KUMAR[2] †

[1]Laboratoire de Mécanique, Université du Havre, 25 rue Philippe Lebon, 76058 Le Havre cedex, France

[2] Laboratoire de Physique Statistique, Ecole Normale Supérieure, 24 rue Lhomond, 75231 Paris cedex 05, France

(Received 15 June 1999 and in revised form 13 March 2000)

Instabilities of a wake produced by a circular cylinder in a uniform water flow are studied experimentally when viscoelastic solutions are injected through holes pierced in the cylinder. It is shown that the viscoelastic solutions fill the shear regions and drastically modify the instabilities. The two-dimensional instability giving rise to the Kármán street is found to be inhibited: the roll-up process appears to be delayed and the wavelength of the street increases. The wavelength increase obeys an exponential law and depends on the elasticity number, which provides a ratio of elastic forces to inertial forces. The three-dimensional instability leading to the A mode is generally found to be suppressed. In the rare case where the A mode is observed, its wavelength is shown to be proportional to the wavelength of the Kármán street and the streamwise stretching appears to be inhibited. Injection of viscoelastic solutions also decreases the aspect ratio of the two-dimensional wake, and this is correlated with stabilization of the A mode and with changes in the shape of the Kármán vortices. The observations of this work are consistent with recent numerical simulations of viscoelastic mixing layers. The results suggest mechanisms through which polymers inhibit the formation of high-vorticity coherent structures and reduce drag in turbulent flows.

## 1. Introduction

For the last 50 years, it has been well known that the addition of small amounts of polymer can drastically change the properties of turbulent flows. However, modifications such as the drag reduction effect (Toms 1948) or the suppression of small-scale fluctuations (McComb, Allan & Greated 1977; Tong, Goldburg & Huang 1992) are still not well understood. Indeed, the link between these two phenomena remains especially unclear (Cadot, Bonn & Douady 1998). While it is clear that there is a strong polymer–flow interaction (Hinch 1977), the mechanisms through which polymers modify turbulence still remain an open issue, partly due to the uncertainty about the way in which small-scale turbulence is generated (Sreenivasan & Antonia 1997). One fruitful approach to studying turbulent flows has been to focus on the behaviour of prototypical coherent structures, an example of which is vorticity filaments. The

† Present address: Department of Chemical Engineering, University of Michigan, 2300 Hayward, 3074 H.H. Dow Building, Ann Arbor, MI 48105 USA.

goal of this work is to gain some insight into how the addition of polymer affects the formation of vorticity filaments. We pursue this by studying experimentally the effect of polymer injection on the instabilities of a wake produced by uniform water flow past a circular cylinder.

Experiments (Douady, Couder & Brachet 1991; Villermaux, Sixou & Gagne 1995) and numerical simulations (e.g. Siggia 1981; Kida & Miura 1998; Jimenez & Wray 1998) during the last 20 years have demonstrated the existence of rare, but intense, small-scale vorticity structures of tube- and sheet-like shapes in turbulent flows. A mechanism for the production of such vorticity structures, which we refer to as vorticity filaments, was conjectured by Douady *et al.* (1991), and then refined by Cadot, Douady & Couder (1995) on the basis of pressure fluctuation measurements. The filaments are thought to form from vorticity layers which are being strained along the vorticity direction. Further support for this idea comes from numerical simulations by Passot *et al.* (1995) showing that instability of a vorticity layer under strain concentrates the vorticity into a steady tubular structure. In the model proposed by Cadot *et al.* (1995), concentration of vorticity into filaments can occur at any scale of the turbulence, the vorticity layer being produced and stretched by a larger structure. This mechanism is very similar to what is observed in secondary instabilities of mixing layers (Bernal & Roshko 1986) and body wakes (Williamson 1996*a*), or in the recent experiment of Leweke & Williamson (1998*a*) studying the interaction of two counter-rotating vortices. In these flows, small-scale vorticity layers are produced by a three-dimensional instability of the primary spanwise rolls. The dynamics of vorticity concentration is then governed by the straining flow between the rolls, as first discussed by Lin & Corcos (1984) and Neu (1984).

The effect of polymer additives on the formation of vorticity filaments has been a subject of recent investigations. Bonn *et al.* (1993) injected a polymer solution into a fully turbulent flow and found that filament formation was partially inhibited. This observation was then confirmed by Cadot *et al.* (1998), but was found to be valid only during the time that the semi-dilute polymer solution was being mixed into the turbulent flow. Thus, the effect of filament inhibition is a form of heterogeneous drag reduction (Vleegaar & Tels 1973; Bewersdorff *et al.* 1993), where the injected polymer solution behaves like a coherent viscoelastic thread.

Theoretical work related to filament inhibition by polymers has been carried out in several different areas. The filament formation process is thought to involve mechanisms similar to instabilities in mixing layers, flows in which viscoelastic effects have been addressed. Azaiez & Homsy (1994) studied the two-dimensional roll-up instability of a mixing layer using the Oldroyd-B constitutive model. Their linear analysis revealed a shift to lower growth rates and longer wavelengths as the ratio of elastic forces to inertial forces increased. Recent experiments based on the visualization of a wake past a circular cylinder appear to be consistent with these predictions (Cadot & Lebey 1999). Numerical simulations of instability in two- and three-dimensional mixing layers were performed by Kumar & Homsy (1999), who used the FENE-P constitutive model. They demonstrated that small changes to the two-dimensional roll-up process produce only small changes in the stability of the primary spanwise rolls to three-dimensional perturbations, relative to the Newtonian case. Their work also suggested that by modifying the two-dimensional roll-up, polymers could stabilize the flow to three-dimensional perturbations. Turbulent channel flow is relevant to filament formation as well, and direct numerical simulations using the FENE-P model have been carried out by Sureshkumar, Beris & Handler (1997). Compared to Newtonian liquids, they find weaker streamwise vorticity fluctuations and an increase in the

spacing of streamwise streaks of low-speed fluid. These observations are consistent with experiments and suggest that the near-wall streamwise vortices (which are analogous to vorticity filaments) are less intense. Finally, Yarin (1997) has presented an analysis of a vortex filament being stretched by a shear flow in a dilute polymer solution. The presence of polymer is found to retard filament stretching, making it difficult to generate hairpin-like configurations which may then break down and produce small-scale turbulence.

Since the three-dimensional instability of the primary spanwise rolls in mixing layers and body wakes is relevant to understanding the mechanism through which vorticity filaments are formed, we study here the effect of polymer injection on the wake of a cylinder. In Newtonian fluids, these wakes have been extensively studied and are known to undergo a sequence of instabilities leading to turbulence (Berger & Wille 1972; Williamson 1996*a*). At a Reynolds number ($Re$) of $\sim 50$, the basic flow is susceptible to a two-dimensional instability which produces the well-known Kármán vortex street ($Re$ here is based on the free-stream velocity and cylinder diameter). At higher $Re$, two distinct types of three-dimensional instabilities can set in. In the range $170 < Re < 250$, the instability takes the form of an undulation in the Kármán rolls just behind the cylinder and is referred to as mode A. This undulation leads to the formation of vorticity sheets separated by a typical length of 3–4 cylinder diameters. The sheets then roll up into longitudinal vortex filaments which form loops around the primary Kármán rolls. For $Re > 250$, the three-dimensional instability has a different character and is known as mode B. Here, streamwise vortices develop in the shear layer connecting the primary Kármán rolls to the cylinder and have a typical spacing of about 1 cylinder diameter (Leweke & Williamson 1998*b*).

Existing studies of polymeric liquid flow past cylinders can be divided into two main groups. The first consists of studies at $Re < 50$, where the Kármán instability does not set in. The aim of these works is to investigate either purely elastic instabilities (e.g. Shiang *et al.* 1997 and references therein) or anomalous transport properties (James & Acosta 1970; Mizushina & Usui 1975; Konuita, Adler & Piau 1980). The latter refers to the observation that above a certain value of $Re$, the Nusselt number and the drag coefficient become essentially constant. This is due to the formation of a region of slow-moving fluid behind the cylinder, and is believed to be a consequence of a 'change of type' in the vorticity equation from elliptic to hyperbolic (Delvaux & Crochet 1990; Joseph 1990). The second group of studies deals with the effects of polymer additives on vortex shedding. For relatively low $Re$ ($\sim 100$), additives are found to reduce the shedding frequency (Kalashnikov & Kudin 1970; Usui, Shibata & Sano 1980), but at much higher $Re$ ($\sim 10^4$), the shedding frequency is not significantly different from the Newtonian case (Sarpkaya, Rainey & Kell 1973; Kim & Telionis 1989).

While flow visualizations show the strong effect of polymer additives on turbulent mixing layers (Hibberd, Kwade & Scharf 1982; Riediger 1989), we are not aware of any experiments which study viscoelastic effects on three-dimensional laminar instabilities in either mixing layers or body wakes. We address this issue in the present work. In § 2, we describe our experimental setup, measurements, and analysis. The results presented in § 3 further quantify the two-dimensional observations of Cadot & Lebey (1999), and present new information about the two- and three-dimensional instabilities as well. The results are discussed in § 4, along with their possible implications for filament inhibition and turbulent drag reduction. Finally, we conclude in § 5.

## 2. Experiment

### 2.1. *Apparatus*

The experiment has already been described in detail by Cadot & Lebey (1999); only minor changes to the injection system and the cylinder geometry are described here. The main water flow is produced by gravity in a vertical channel with a constant level system. The test channel has a cross-section of 200 mm $\times$ 150 mm and a length of 600 mm. A circular tube (the cylinder) with a 4 mm diameter is placed horizontally. Two oblique end plates are added on both sides in order to minimize end effects. The tube is pierced with two parallel rows of 67 holes, each hole having a diameter of $0.55 \pm 0.05$ mm. The distance between two consecutive holes is 2 mm. The two rows form an angle of 90° with respect to the centreline of the tube, and they are oriented upstream and symmetrically with respect to the main flow. This setup is clearly observable in all the pictures in this article, and especially in figures 5 and 10 where coloured solution exits the holes. The solution is injected using a peristaltic pump, where the injection rate is simply imposed by the rotation frequency of the pump. The advantage of such a pump is that the injection rate does not depend on the solution viscosity. An inconvenience is that the solution is periodically pulsed due to the pinching of the flexible tubes which deliver the injected solution. To deal with this, we insert a 250 ml container partially filled with air between the pump and the cylinder. For a sufficiently large amount of air, the high-frequency pulsations are removed. Even though there is a risk that the solution may be fractionated by the pump and then potentially degraded, we did not observe any significant changes from the case of gravity-driven smooth injection used in the preliminary study of Cadot & Lebey (1999). We define the Reynolds number of the experiment using the mean velocity of the uniform main water flow, $U$, the viscosity of water, $\nu$, and the cylinder diameter, $d$: $Re = Ud/\nu$. The precision of the Reynolds number is about 5%. We also define an injection parameter $\beta = u/U$, where $u$ is the mean velocity through the injection holes. The parameter $\beta$ is representative of the fraction of fluid in the vicinity of the cylinder which has been injected. The value of $u$ is simply computed from the known injection rate of the pump and the total surface area of injection; its maximum value is $6.8\,\mathrm{cm\,s^{-1}}$. The maximum $Re$ we can reach is $Re \sim 300$ for $U \sim 7\,\mathrm{cm\,s^{-1}}$.

### 2.2. *Injected solutions*

The viscoelastic solutions are made from water and WSR 303 polyethyleneoxide (PEO; from Union Carbide). The molecular weight of the WSR 303 (based on rheological measurements) as reported by the manufacturer is $7 \times 10^6\,\mathrm{g\,mol^{-1}}$. We perform experiments with several different solution concentrations, from 100 w.p.p.m. to 1000 w.p.p.m. Shear viscosity measurements of the solutions (made using a Contraves Low-Shear 30 rheometer) are displayed in figure 1. A strong shear-thinning behaviour is observed as the shear rate increases. In addition, these solutions are known to exhibit elastic properties which manifest themselves in a non-vanishing first normal stress difference (Vissman & Bewersdorff 1990). In order to extract a time constant related to this elasticity, we fit the shear viscosity data with the Carreau model (Bird, Armstrong & Hassager 1987*a*):

$$\eta = \eta_0(1 + (\tau\dot{\gamma})^2)^{-N}. \tag{2.1}$$

The zero-shear viscosity $\eta_0$, Carreau time constant $\tau$, and exponent $N$ are reported in table 1 for each solution concentration. From these data, the intrinsic viscosity

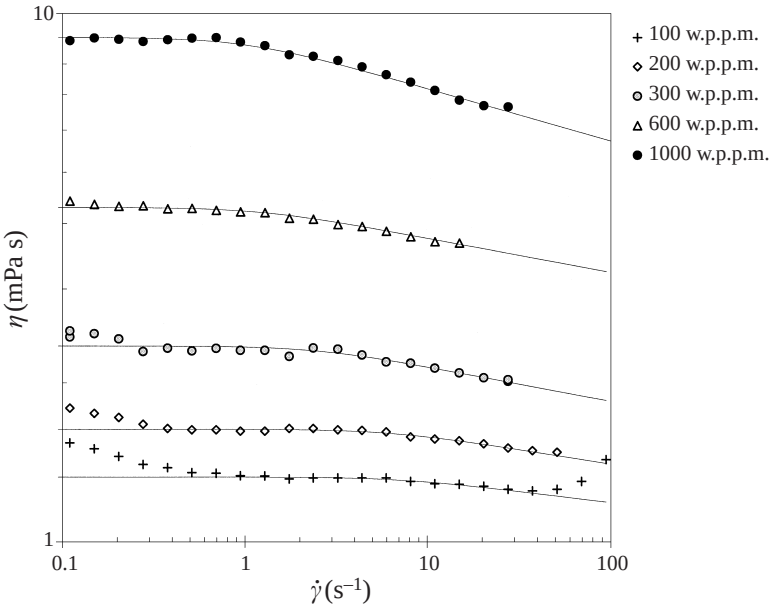


FIGURE 1. Measurements of the shear viscosity versus the shear rate for the WSR 303 PEO solutions. The solid lines are fits of the Carreau model, $\eta = \eta_0(1 + (\tau\dot{\gamma})^2)^{-N}$, and the resulting parameters are reported in table 1.

| Concentration (w.p.p.m.) | $\eta_0$ (mPa s) | $\tau$ (s) | $N$ |
|---|---|---|---|
| 100 | 1.32 | 0.13 | 0.022 |
| 200 | 1.63 | 0.15 | 0.028 |
| 300 | 2.34 | 0.4 | 0.033 |
| 600 | 4.28 | 0.8 | 0.033 |
| 1000 | 9 | 0.98 | 0.049 |

TABLE 1. Parameters of the Carreau model, $\eta = \eta_0(1 + (\tau\dot{\gamma})^2)^{-N}$, for the WSR-303 PEO solutions.

$[\eta_0]$ can be computed by a linear extrapolation of the reduced viscosity to zero concentration (Bird *et al.* 1987*a*):

$$[\eta_0] = \lim_{c \to 0} \frac{\eta - \eta_{water}}{c\eta_{water}} = 0.0024 \text{ w.p.p.m.}^{-1}. \tag{2.2}$$

The overlap concentration, $c^*$, which marks the transition from a dilute to a semi-dilute solution (Doi & Edwards 1986), is estimated by two methods. The first is the intersection of the low- and high-concentration asymptotes on a plot of the zero-shear viscosity versus concentration. The second is Graessley's formula based on the intrinsic viscosity, $c^* = 0.77/[\eta_0]$ (Graessley 1980; Vlassopoulos & Schowalter 1994). In each case, we find an overlap concentration of around 320 w.p.p.m. Hence, some of our solutions (600 and 1000 w.p.p.m.) have to be considered semi-dilute. In semi-dilute solutions, individual polymer molecules begin to overlap each other and can form large supermolecular aggregates like micronetworks (Georgelos & Torkelson 1988). The viscoelastic properties are then not only directly related to the

concentration of the solution, but also to the organization of the aggregates. As a consequence, estimates of relaxation times based on the dilute-solution models of Rouse and Zimm (Bird *et al.* 1987*b*), tend to be much smaller than time constants (e.g. Carreau) based on shear-thinning curves (see Vlassopoulos & Schowalter 1994 for a detailed comparison). Thus, the latter time constants should not be interpreted as relaxation times of individual polymer chains.

To perform experiments at different Reynolds numbers and injection rates, 51 of solution is needed at each concentration. For a given solution, all measurements are performed over one day. Six different Reynolds numbers and fifteen different injection rates are explored for each solution, and we wait 5 min for the flow to stabilize after modification of the control parameters. The main difficulty in these experiments is that the viscoelastic properties of such large amounts of solution are sensitive to the way in which the solutions are prepared, and could be non-homogeneous in a given solution. This is due to the formation of aggregates, as mentioned above. This kind of inhomogeneity is a problem because we would like the prepared solution to have the same viscoelastic properties during an experiment in which $Re$ and $\beta$ are varied. In addition, flow-induced degradation of the aggregates could occur (Hinch & Elata 1979). We had difficulties with some prepared solutions, and the more coherent quantitative results of wavelength measurements were obtained with solutions of concentrations 250 w.p.p.m., 600 w.p.p.m., and 1000 w.p.p.m. Results are also shown for a 500 w.p.p.m. solution, but the reproducibility with Reynolds number and injection rate is not as good.

### 2.3. *Measurements and analysis*

The wake is recorded with a standard digital CCD video camera. The injected solutions are coloured with crystal violet and the wake is illuminated from behind. The camera field contains the cylinder and the axes of the Kármán rolls, allowing us to make measurements of the wavelength of the Kármán street and the three-dimensional instabilities. In a typical experimental run, the wake is recorded for 1 min for given values of $Re$ and $\beta$. The data are then initially analysed on a monitor in order to extract some representative pictures for wavelength measurements. These pictures are transferred to a PC via the acquisition board Imaq 1408 and then processed using the Labview software. Since the pictures are never completely two-dimensional, the two-dimensional wavelength $\lambda$ is simply determined by eye through measurement of many (locally perpendicular) distances between two consecutive Kármán rolls. We then extract a mean value along with its typical fluctuation. Another treatment, completely automatic and in real time, is to take an intensity line perpendicular to the cylinder in the camera field. Each Kármán roll is then localized by a maximum of intensity, and a simple analysis of the peak periodicity gives the local wavelength in time and in space. The disadvantage of this technique is that it requires a nice bi-dimensional wake. For example, in the case of oblique vortex shedding (Williamson 1989), the wavelength is obviously overestimated (see figure 2). On the other hand, this treatment allows us to estimate an average wavelength over thousands of local measurements, which results in converged values. The three-dimensional wavelength, $\Lambda$, is measured directly by eye.

Side views of the wake have also been taken in order to visualize the shape of the Kármán vortices and the aspect ratio of the wake, $k = h/\lambda$, where $\lambda$ is the distance between two consecutive co-rotating vortices and $h$ is the vertical separation between the two rows of counter-rotating vortices. For these experiments, the injected solutions are coloured with fluorescent dye and the wake is illuminated by a light sheet. In a

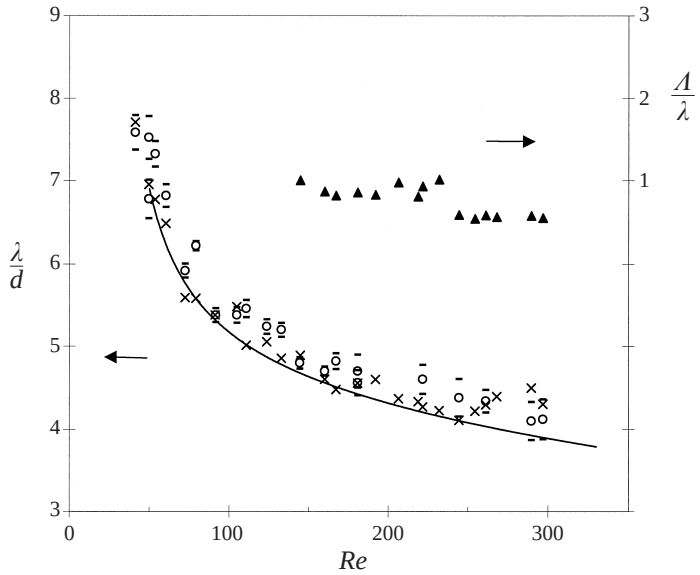


FIGURE 2. Wavelength measurements versus the Reynolds number in the case of water injection. The wavelength of the two-dimensional instability is denoted by $\lambda$, and the cylinder diameter by $d$. Crosses: measurements of $\lambda$ from distances locally perpendicular to the Kármán rolls. Open circles: measurements of $\lambda$ from distances perpendicular to the cylinder. Notice that the second set of measurements is systematically overestimated due to the oblique vortex shedding. The solid line is the space-equivalent Williamson (1989) formula for parallel vortex shedding (see equation (3.1)). Solid triangles: measurements of the three-dimensional wavelength, $\Lambda$.

few pictures of the Kármán street, the aspect ratio has been measured at different locations in the wake to show the evolution of the aspect ratio with the downstream distance from the cylinder.

## 3. Results

We first present general observations about the effects of water and PEO injection, then give details separately about the two- and three-dimensional instabilities.

### 3.1. *Water injection – general effects*

Figure 2 shows the wavelength measurements in the case of water injection. We use the lowest injection rate allowing a sufficient visualization for these measurements; $\beta$ never exceeds 0.1. The continuous line is the space-equivalent formula proposed by Williamson (1989) for parallel shedding:

$$\lambda = \frac{\alpha U}{f} \quad \text{with} \quad S = \frac{fd}{U} = -\frac{3.22}{Re} + 0.18 + 1.610^{-4} Re. \tag{3.1}$$

where $f$ is the shedding frequency of the Kármán vortices and $S$ is the Strouhal number.

The phase velocity $\alpha U$ of the Kármán rolls was estimated from local measurements of frequency shedding and wavelength to be $0.85U$. From figure 2, we observe good agreement between our data and Williamson's formula. For $150 < Re < 250$, the three-dimensional instability appears as a pure A mode, while for higher $Re$,

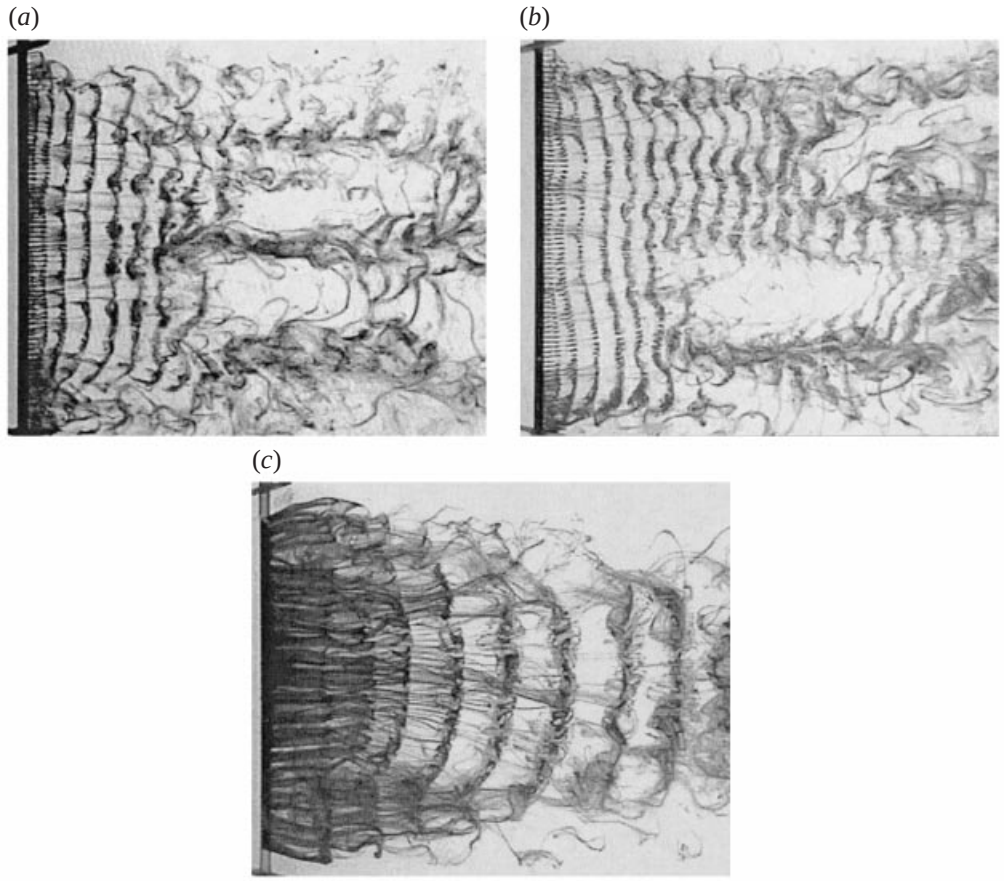


FIGURE 3. Visualization of the wake for three similar cases at a large injection rate ($\beta \sim 0.6$) of (*a*) water; and PEO solution with concentration, (*b*) 250 w.p.p.m. and (*c*) 1000 w.p.p.m. The velocity of the flow is $U = 4.8\,\mathrm{cm\,s^{-1}}$ ($Re \sim 190$).

other three-dimensional instabilities manifest themselves. This explains the jump in the ratio of the spanwise to streamwise wavelengths, $\Lambda/\lambda$, from $\sim 1$ to $\sim 0.5$ at $Re \sim 250$. In the experiments reported here, we focus our attention on the A mode of the three-dimensional instability. A discussion of other three-dimensional instability modes in wakes behind circular cylinders can be found in Zang *et al.* (1995), Brede, Eckelmann & Rockwell (1996) and Williamson (1996*a*). A problem in the measurement of $\Lambda$ is that the A mode is not stable in time and in space, meaning that the periodic patterns like those presented in figure 11 are transient. Most of the time, the dye sheets are continuously formed and destroyed (see figures 10*a* and 10*b*). To deal with this, we measured the wavelength only when more than two sheets were present in the wake and separated by equivalent distances. Our wavelength measurements of the A mode shown in figure 2 are in agreement with previous measurements by Zang *et al.* (1995), Brede *et al.* (1996) and Williamson (1996*b*), who found wavelengths of three to five times the cylinder diameter. The fact that the ratio $\Lambda/\lambda$ is almost constant suggests that the wavelength of the three-dimensional instability is based on the wavelength of the Kármán street.

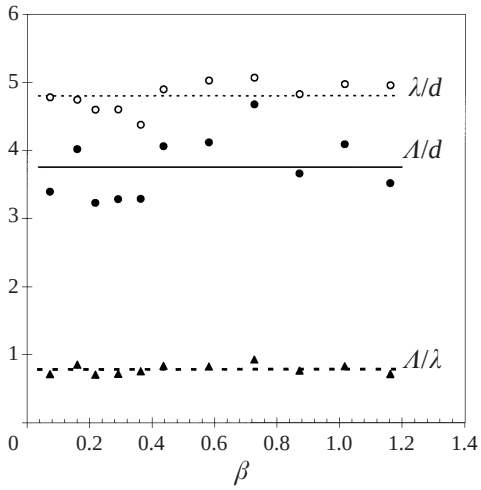


FIGURE 4. Effects of water injection on the two- and three-dimensional wavelengths ($\lambda$ and $\Lambda$, respectively) at $Re \sim 170$. The cylinder diameter is denoted by $d$. Both wavelengths are independent of the injection rate, $\beta$. This is also observed at other values of the Reynolds number, up to $Re \sim 300$. Note that the wavelength ratio is less dispersed than the wavelength measurements themselves.

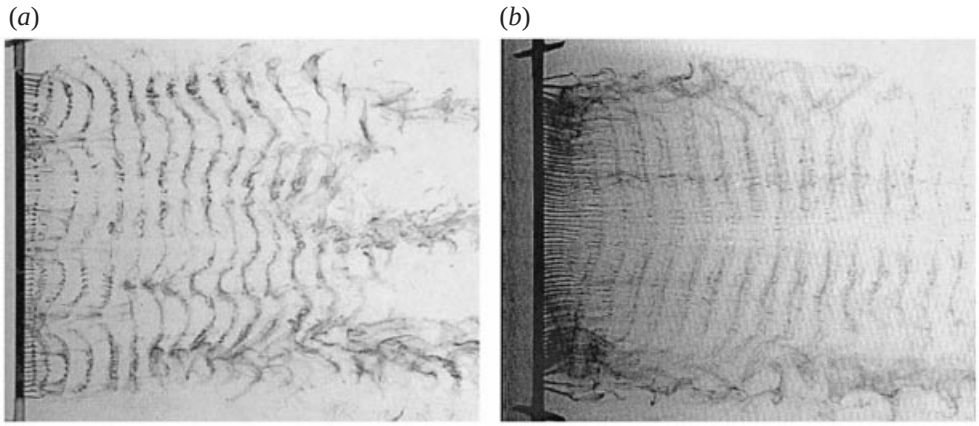


FIGURE 5. Visualization of the wake for two similar cases at a low injection rate ($\beta \sim 0.05$) of (*a*) water, and (*b*) 1000 w.p.p.m. PEO solution. The velocity of the flow is $U = 4.8\,\mathrm{cm\,s^{-1}}$ ($Re \sim 190$). We can observe that even for this low injection rate, the three-dimensional disturbance seen in (*a*) is drastically suppressed in (*b*).

### 3.2. *PEO injection – general effects*

Figures 3, 5, and 6 are representative of the effects produced on the wake by injection of the PEO solutions.

In figure 3, only the concentration of the injected solutions is changed; the velocity of the flow is $4.8\,\mathrm{cm\,s^{-1}}$ ($Re \sim 190$) with the injection parameter $\beta \sim 0.6$. Figure 3(*a*) shows the reference Newtonian case, where the parallel vortex shedding and the A mode are clearly observable. For a PEO concentration of 250 w.p.p.m., neither the two- nor three-dimensional wavelengths are strongly affected (figure 3*b*). But when the PEO concentration is 1000 w.p.p.m., the two-dimensional wavelength is spectacularly increased (at this value of $\beta$) and the A mode disappears (figure 3*c*). These effects

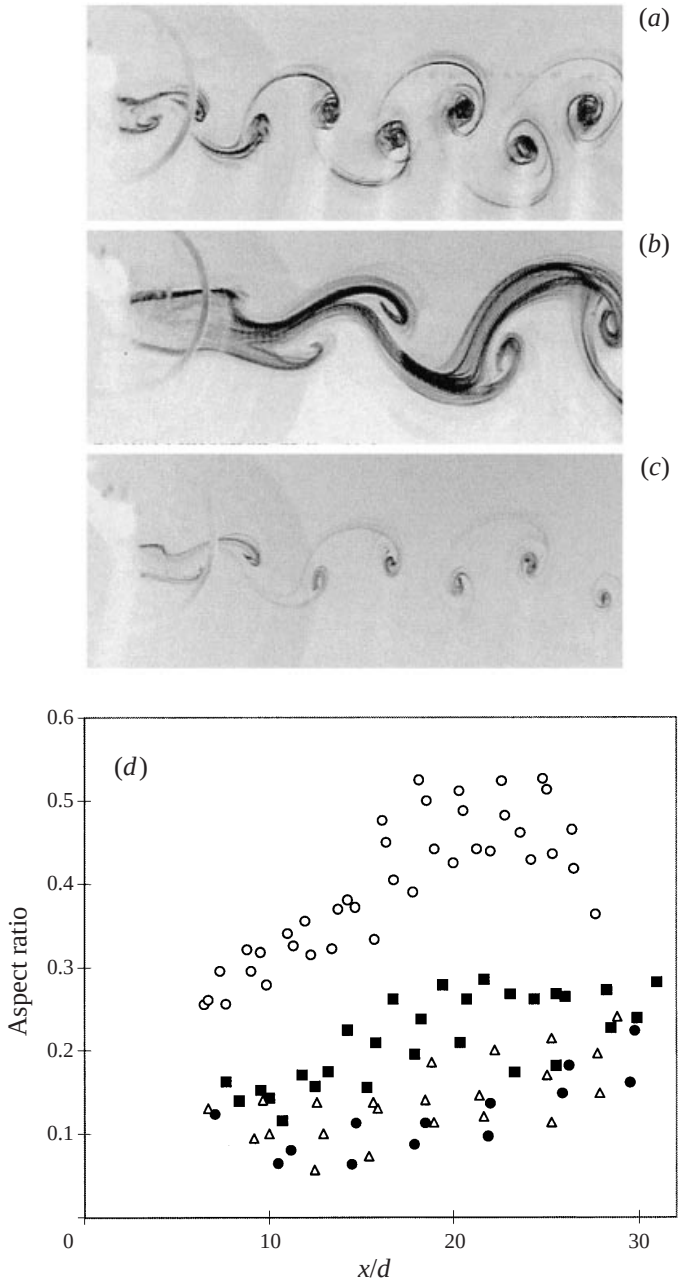


FIGURE 6. Visualization of the Kármán street for injection of (*a*) water at $\beta \sim 0.5$, and PEO solution with concentration 600 w.p.p.m. at (*b*) $\beta \sim 0.5$, and (*c*) $\beta \sim 0.05$. The velocity of the flow is $U = 3.75\,\mathrm{cm\,s^{-1}}$ ($Re \sim 150$). (*d*) Measurements of the aspect ratio of the wake versus the distance downstream for injection of water (open circles) at $\beta \sim 0.5$ and a 1000 w.p.p.m. PEO solution at $\beta \sim 0.5$ (filled circles); $\beta \sim 0.1$ (open triangles); $\beta \sim 0.05$ (filled squares). The cylinder diameter is denoted by $d$.

cannot be related to a perturbation of the boundary layer caused by the injection jet. As shown in figure 4, with simple water injection the two- and three-dimensional wavelengths remain relatively constant as the injection parameter increases.

Figure 5 shows the case of a very low injection rate ($\beta \sim 0.05$) for water and the 1000 w.p.p.m. PEO solution. As in figure 3, $Re \sim 190$. It is remarkable that while the two-dimensional wavelength is not significantly affected by the polymer solution, the three-dimensional perturbation is clearly suppressed.

Figure 6 shows a side view of the wake at low and high injection rates for $Re \sim 150$. We can observe, in addition to the two-dimensional wavelength increase, a drastic change in the shape of the Kármán street at both injection rates of the 1000 w.p.p.m. PEO solution. Comparison of figures 6(*b*) and 6(*c*) (PEO injection) to figure 6(*a*)(water injection) suggests that PEO injection causes a decrease in the aspect ratio of the wake. This result is given more quantitatively in figure 6(*d*), which shows local measurements of the aspect ratio (see § 2.3). In the case of water injection, the aspect ratio assumes a minimum value of 0.3 at the beginning of the wake. This value increases downstream due to the three-dimensional disturbances of the wake. The results for water injection are found to be essentially independent of $\beta$. As the injection of rate of the 1000 w.p.p.m. solution increases, the minimal value of the aspect ratio decreases continuously to a value of 0.1. Once again it is important to notice that at low injection rates, these effects occur without significant changes to the wavelength of the two-dimensional instability. Another important observation is that for large injection rates, some polymer solution remains in the braid region between the rolls (figure 6*b*). A final observation is the presence of a large zone of slow fluid motion just behind the cylinder (figures 6*b* and 6*c*) which increases in size as the injection rate (or the concentration of the solution) increases.

### 3.3. *PEO injection – two-dimensional instability*

Measurements of the Kármán street wavelength are shown in figure 7 for injection of water, and the 600 and 1000 w.p.p.m. PEO solutions. In the case of the 600 w.p.p.m. solution, we observe that the wavelength increases as the injection parameter increases and then saturates to a maximum value. The initial values at $\beta = 0$ correspond to the wavelengths measured in the case of water injection. We detected no threshold value of $\beta$ which is required for the wavelength increase. Similar behaviour is seen with the 1000 w.p.p.m. solution, but the saturation wavelengths are larger. Indeed, we have observed this generic behaviour for all the solutions with concentrations greater than 250 w.p.p.m. over the range of $Re$ we have explored. For a 250 w.p.p.m. solution, no measurable effect can be discerned due to the large dispersion in the wavelength measurements. In order to extract a generic law from the data in figure 7, we computed the dimensionless wavelength increase as $(\lambda - \lambda_o)/\lambda_o$ where $\lambda_o$ is the wavelength measured for water injection at a given $Re$. We then fit all the experimental data with a simple exponential law having two adjustable parameters, $\lambda_{sat}$ and $\beta^*$:

$$\frac{\lambda - \lambda_o}{\lambda_o} = \frac{\lambda_{sat} - \lambda_o}{\lambda_o}(1 - \exp[-\beta/\beta^*]). \tag{3.2}$$

The quantity $\beta^*$ can be interpreted as the characteristic fraction of viscoelastic solution in the vicinity of the cylinder needed to reach the saturation value, $\lambda_{sat}$, whereas $1/\beta^*$ is the slope of the fitted curve at low values of the injection parameter. In figure 8, we can see that all the data collapse onto the exponential-law curve. The values obtained for $\beta^*$ and $(\lambda_{sat} - \lambda_o)/\lambda_o$ are plotted in figures 9(*a*) and 9(*b*). In figure 9(*a*), the data are displayed in terms of the Weissenberg number of the experiment,

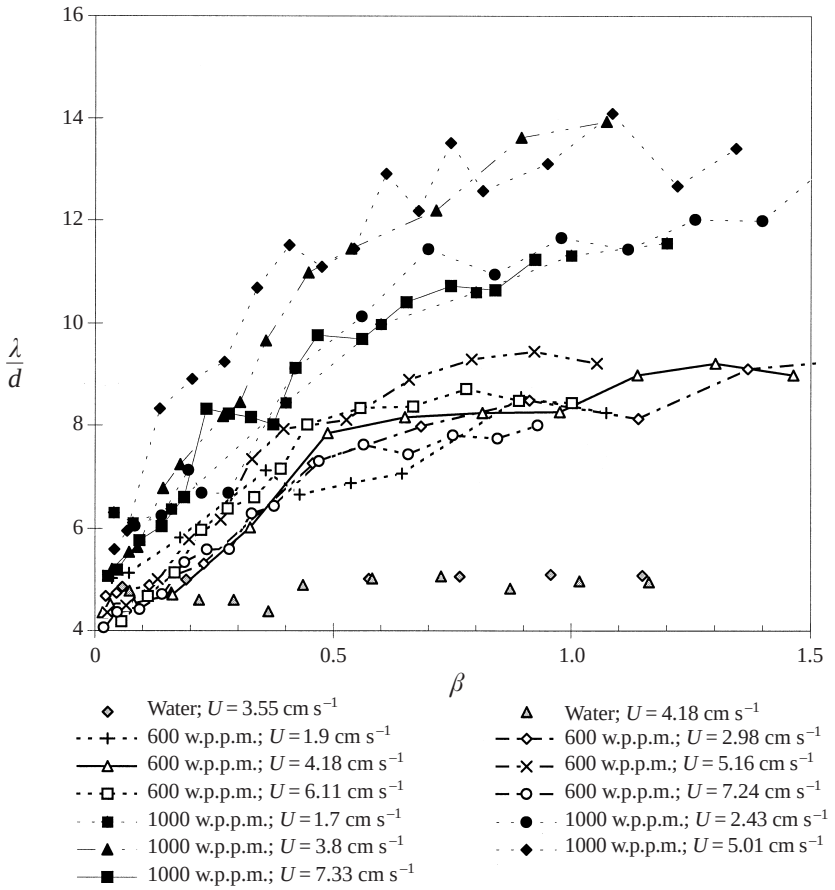


FIGURE 7. Measurements of the two-dimensional wavelength, $\lambda$, versus the injection parameter, $\beta$, for different velocities of the main flow (i.e. $Re$) and different solution concentrations. The cylinder diameter is denoted by $d$. Grey symbols: water injection. Open symbols: injection of the 600 w.p.p.m. PEO solution. Filled symbols: injection of the 1000 w.p.p.m. PEO solution. The maximum velocity $U$ corresponds to $Re \sim 300$ and the minimum to $Re \sim 70$.

defined as

$$We = \frac{\tau U}{d}, \tag{3.3}$$

where $\tau$ is the Carreau time constant (table 1). The dimensionless wavelength increase at saturation, $(\lambda_{sat} - \lambda_o)/\lambda_o$, appears to depend on both the concentration of the injected solutions and $We$. The larger the concentration, the larger the dimensionless wavelength increase at fixed $We$. A similar behaviour is found at fixed concentration with respect to $We$, but a maximum is displayed followed by a decrease. The value of $We$ where the dimensionless wavelength increase is maximum is similar for the two solutions. In contrast, $\beta^*$ does not seem to depend on the nature of solution but it does tend to decrease with $U$.

### 3.4. *PEO injection – three-dimensional instability*

For injections at concentrations lower than 250 w.p.p.m., the A mode is as persistent as it is in the Newtonian case and no measurable changes in its properties are

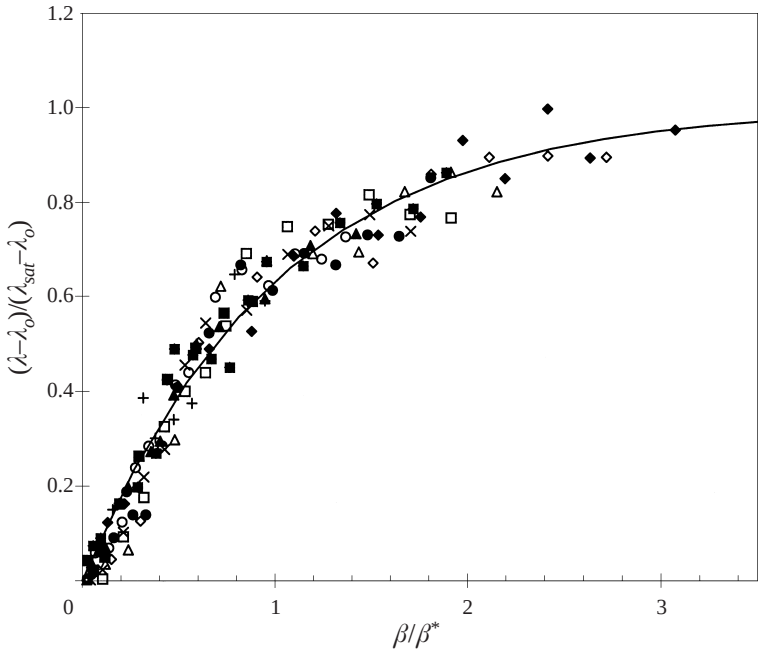


FIGURE 8. The experimental data of figure 7 in terms of the coordinates suggested by equation (3.2). The solid line is the curve given by $(\lambda-\lambda_o)/(\lambda_{sat}-\lambda_o)=1-\exp[-\beta/\beta^*]$. Values of $\lambda_{sat}$ and $\beta^*$ can be found in figure 9. The wavelength measured for water injection at a given Reynolds number is $\lambda_o$.

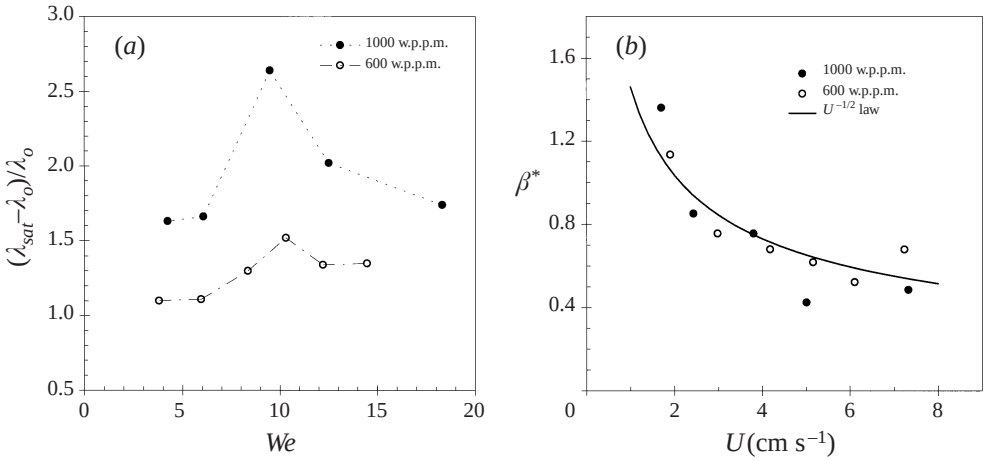


FIGURE 9. (*a*) The dimensionless increase in the saturated two-dimensional wavelength ($\lambda_{sat}$) versus the Weissenberg number. The wavelength measured for water injection at a given Reynolds number is $\lambda_o$. (*b*) The characteristic injection parameter, $\beta^*$, versus the velocity of the main flow, $U$.

observed over the range of $Re$ and $\beta$ we examined. For higher concentrations, we generally find that development of the A mode is damped even at very low injection rates. An example of this is seen in figures 3(*c*) and 5(*b*). In figure 3(*c*), the injection rate is large enough so that the two-dimensional wavelength increases. In figure 5(*b*), the A mode is also damped but $\beta$ is too small to cause a measurable change in the

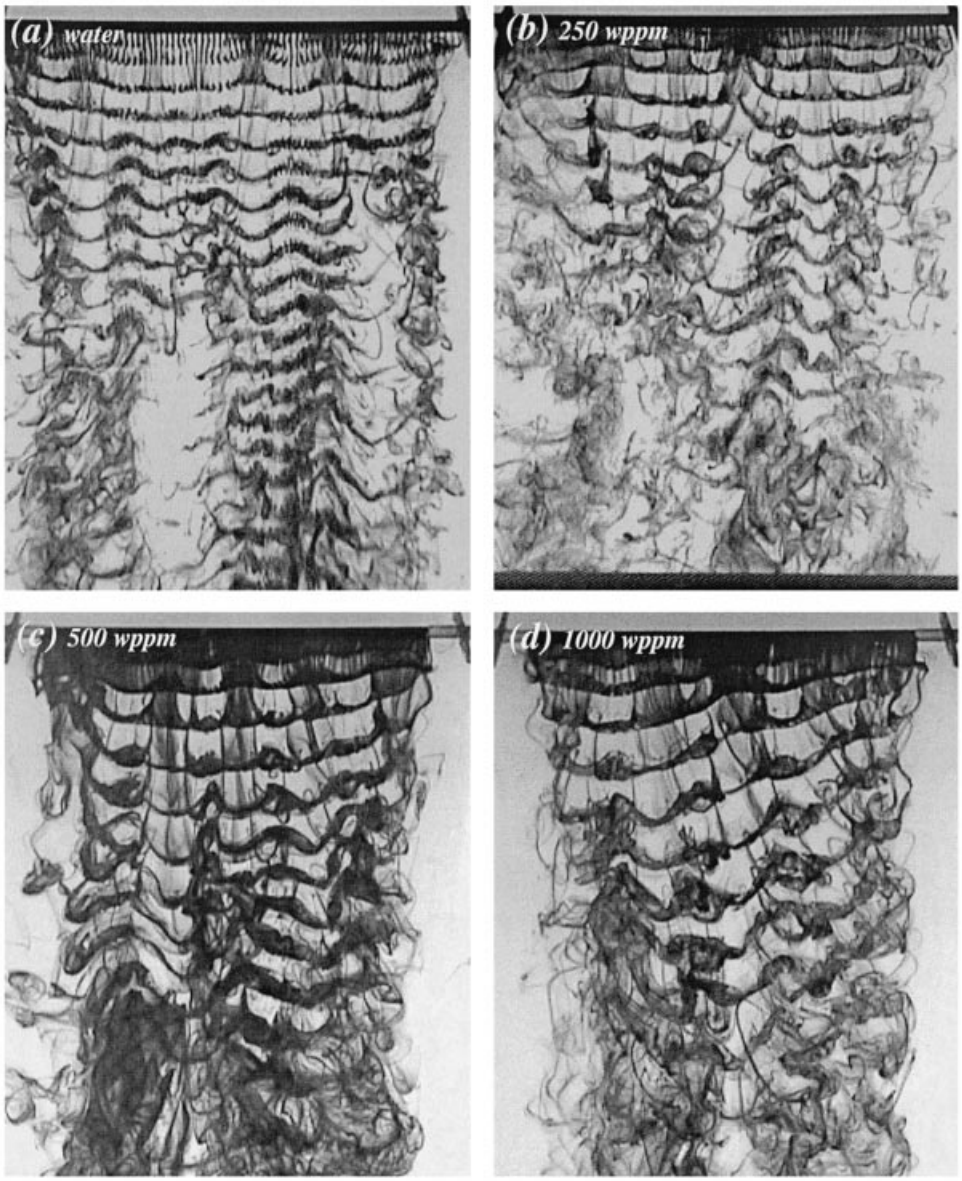


FIGURE 10. Visualization of the wake during the observation of the three-dimensional instability (A mode) for injection of (*a*) water at $Re \sim 170$; and PEO solution with concentration, (*b*) 250 w.p.p.m. at $Re \sim 200$, (*c*) 500 w.p.p.m. at $Re \sim 140$, and (*d*) 1000 w.p.p.m. at $Re \sim 140$. In each of the cases of PEO injection, the injection rate is such that the 2D wavelength has almost saturated.

two-dimensional wavelength. Even though the A mode is usually damped in the high-concentration solutions, we find that it can appear on rare occasions. Figure 10(*a–d*) shows the A mode when water and polymer solutions of different concentrations are injected. (The values of $\beta$ are such that the two-dimensional wavelength has almost saturated.) For polymer concentrations greater than 250 w.p.p.m., both the two- and three-dimensional wavelengths increase. This is more clearly seen in figure 11, where the pictures of figure 10 have been rescaled by their two-dimensional wavelength ($\lambda$)

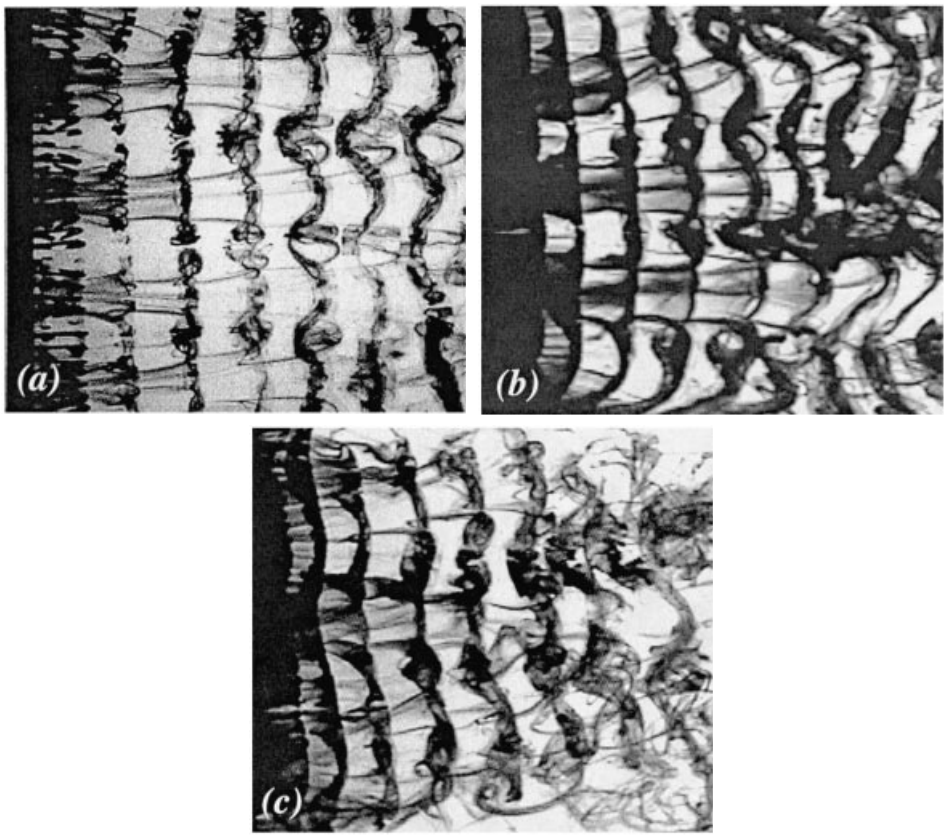


FIGURE 11. Pictures of the A mode from figure 10 non-dimensionalized by the two-dimensional wavelength, $\lambda$, for injection of (*a*) water, $\lambda = 4.5d$; and PEO solutions with concentrations, (*b*) 500 w.p.p.m., $\lambda = 9d$, and (*c*) 1000 w.p.p.m., $\lambda = 13d$. The cylinder diameter is denoted by $d$. The aspect ratios of the wakes are reasonably conserved while the two-dimensional wavelengths are very different.

in both space directions so that they all have the same streamwise wavelength. In both of the cases of polymer injection, the ratio of the three-dimensional wavelength to the two-dimensional wavelength remains the same as in the Newtonian case.

Several other observations about the three-dimensional instability deserve mention. First, even when the A mode is damped, three-dimensional events like dislocations and single dye sheets are not inhibited by the polymers (e.g. figure 3*c*). Second, whenever polymer solutions are injected, we find many small-scale streamwise streaks like those shown in figure 3(*c*). This is probably not related to the formation of secondary streamwise vortices of a type other than those observed in the A mode since the streaks are absent in the Newtonian case. More likely, the streaks are due to the fact that the flow field coming out of the injection holes is rather extensional in nature. The resulting polymeric jets would then tend to be more coherent than their Newtonian counterparts (Bird *et al.* 1987*a*). Third, when the A mode is present in the viscoelastic case, the streamwise vortices appear to be wider (figure 11). As these tubes form in a typical time $\lambda/U$, their larger thickness in the viscoelastic cases suggests that the streamwise stretching is also being inhibited by the polymers.

## 4. Discussion

### 4.1. *Two-dimensional instability*

The increase in the Kármán wavelength produced by viscoelasticity can be understood in terms of a mechanism involving inhibition of a Kelvin–Helmholtz instability. This has already been pointed out by Cadot & Lebey (1999), who used the linear stability analysis performed by Azaiez & Homsy (1994) for mixing layers which shows that viscoelasticity shifts the instability to longer wavelengths and reduces its growth rates. We can also compare our wavelength increase to the results of Usui *et al.* (1980), who studied vortex shedding in the flow of polymer solutions past a cylinder. They found that a 400 w.p.p.m. PEO solution halved the shedding frequency at $Re \sim 70$, relative to water. This implies a doubling in the wavelength of the Kármán street if the phase velocity remains constant (equation (3.1)). (In our experiments, we found the phase velocity to be relatively independent of injection rate and solution concentration.) A reduced instability growth rate may be manifested in the region of slow-moving fluid near the cylinder (figures 6*b* and 6*c*), whose existence appears to imply that the roll-up has been delayed. However, a second possible explanation for the region of slow-moving fluid is that it is a consequence of a 'change of type' in the vorticity equation (see § 1) (Konuita *et al.* 1980; Delvaux & Crochet 1990). It could be that both of these factors contribute to the size of the region, but we have been unable to determine their relative importance. Nevertheless, the presence of dyed solution in the braid region (figure 6*b*) also suggests that the roll-up is delayed when PEO is present. An insightful physical interpretation of the Kelvin–Helmholtz instability inhibition can be found in an Appendix to Azaiez & Homsy (1994) by Hinch, who shows that the polymers have a stabilizing effect similar to surface tension.

Viscoelastic effects are expected to increase with the elasticity number, $E$, which provides a ratio of elastic forces to inertial forces (Azaiez & Homsy 1994). In our experiments, $E$ can be estimated from the Carreau time constant, $\tau$, the shear viscosity of the solution, $\nu$, and the thickness of the boundary layer on the cylinder, $\delta$: $E \approx \tau\nu/\delta^2$. However, the boundary layer thickness is given by $\delta \approx dRe^{-1/2}$, so we can rewrite $E$ as $E \approx \tau U/d$. This is simply the Weissenberg number (see § 3.3), meaning that $E$ can be interpreted as a local $We$ in these experiments. Looking at figure 9(*a*), we see that the dimensionless wavelength enhancement increases with $We$ before peaking and then decreasing. The increase with $We$ is consistent with the anticipated behaviour. The maximum may occur because shear thinning begins to become important above a certain value of $We$, thereby increasing the relative importance of inertial forces. However, we have been unable to confirm this idea using a modified $E$ which accounts for the shear thinning seen in figure 1. Another possibility for the occurrence of the maximum is that degradation of the macromolecular aggregates may take place if $We$ is too large (Hinch & Elata 1979). We note that the occurrence of the maximum around the value $We \sim 10$ is a consequence of our choice of a time constant. Had we chosen time constants based on the inverse shear rate where the viscosity is 90% of its zero shear value (Vlassopoulos & Schowalter 1994), the maximum would occur closer to $We \sim 1$, the point where shear thinning becomes important (where inertial forces become comparable to elastic forces).

The behaviour of the characteristic injection parameter, $\beta^*$, in figure 9(*b*) can be explained by a simple mechanism. For a given velocity of the main flow, more solution will lie in the vicinity of the cylinder as $\beta$ increases. Since the solution first fills the shear regions (Cadot & Lebey 1999), there will be a characteristic injection parameter, $\beta^*$, where those regions will be completely filled. Increasing $\beta$ beyond $\beta^*$ will not lead

to an additional wavelength increase because the solution will then begin to fill the regions where there is no shear. We expect that $\beta^*$ will scale as the thickness of the shear regions: $\beta^* \sim \delta/d \sim Re^{-1/2}$. This is in agreement with what is observed. As shown in figure 9(*b*), the scaling $\beta^* \sim U^{-1/2}$ is consistent with the experimental data.

It is important to emphasize that the wavelength increase is not simply due to the fact that the polymer solutions have a larger shear viscosity than water. Cadot & Lebey (1999) used a polymer solution with a lower relaxation time (inferred from the lower average molecular weight) but with the same shear viscosity (at the shear rate of interest) as the 1000 w.p.p.m. solution used here. No change from the Newtonian case was seen for the solution with the lower relaxation time, confirming that the wavelength increase observed here is a true viscoelastic effect.

### 4.2. *Three-dimensional instability*

The most remarkable feature of the visualizations involving polymer injection is the damping of the A mode. One possible cause for this damping is that the two-dimensional flow has been modified in such a way that three-dimensional instabilities are more difficult to excite. The decrease in the aspect ratio of the wake when PEO is injected (figure 6*d*) clearly indicates that the polymers are interfering with the two-dimensional base flow. In particular, the results suggest that the growth rates of the A mode become smaller as the aspect ratio of the wake decreases. Intuitively, this is perhaps not surprising since the flow appears more parallel as the aspect ratio decreases. An argument based on the work of Kármán (1911) suggests that the shape of the two-dimensional vortices is modified as well. Kármán (1911) showed that in the inviscid case, two parallel rows of alternating vortices can be stable only for an aspect ratio of $k = 0.28$, independent of the velocity of the flow. From figure 6(*a*), we find a similar value, $k \sim 0.3$, at the beginning of wake in the case of water injection. It is clear from figures 6(*c*) and 6(*d*) that even when $\beta$ is small ($\sim 0.05$), the aspect ratio in the viscoelastic wake is reduced (by about a factor of one-half) relative to the Newtonian case. As a consequence, the shape of the Kármán vortices would have to change in order to maintain a stable wake. Further support is found in figures 6(*a*) and 6(*b*), which show close-ups of the Kármán vortices near the cylinder for injection of water and a 600 w.p.p.m. PEO solution. In the case of PEO injection, the Kármán vortices do not appear to be as well developed.

The above conjectures are consistent with the mixing-layer simulations of Kumar & Homsy (1999). As in the simulations, the three-dimensional instability behaviour does not change much when the two-dimensional instability is unaffected by the polymers (in the experiments, this could correspond to $c < 250$ w.p.p.m.). On the other hand, modification of the two-dimensional flow can inhibit three-dimensional instabilities as suggested by Kumar & Homsy (1999). In their simulations, polymers modified the two-dimensional flow by making it more difficult to collect the vorticity into a single core region, and vortices flatter than those in the Newtonian case resulted. Note that the three-dimensional instability can be inhibited even when the two-dimensional wavelength is unchanged (figure 5). This corresponds to a viscoelastic effect in the nonlinear regime of the instability, which was the case explored in the simulations.

We note several other important issues regarding the three-dimensional instability. First, another possible cause for damping of the A mode may be the presence of the sidewalls. If the addition of polymers increases the three-dimensional wavelength, then increased viscous dissipation at the sidewalls could produce a lower growth rate for the A mode. However, we note that the wavelength of the three-dimensional instability is essentially set by the wavelength of the two-dimensional instability

(figures 10 and 11), and that the three-dimensional instability is damped even if the two-dimensional wavelength is unchanged. Along with the information in figures 5 and 6, this strongly suggests that changes to the two-dimensional flow rather than sidewall effects are responsible for the increased damping. Second, a possible reason for the rare appearance of the A mode may be random disturbances (e.g. flow-rate fluctuations) which accelerate instability growth. As we noted earlier though, the streamwise stretching appears to be inhibited even when the A mode does appear. Third, the fact that the wavelength of the A mode scales as the wavelength of the Kármán street is consistent with what is known about Newtonian wakes. In the Newtonian case, the three-dimensional wavelength is found to be proportional to a length scale characterizing the perturbed two-dimensional flow (Leweke & Williamson 1998*b*). While this length scale is typically identified with the core diameter of the Kármán vortices, it could reasonably correspond to the wavelength of the two-dimensional disturbance. Finally, we again emphasize that the effects we see are not simply related to a viscosity increase. The viscosity of the 1000 w.p.p.m. viscoelastic solution is about 10 times the viscosity of water at zero shear rate, and more than 3 times the viscosity of water at the shear rates in the vicinity of the cylinder. Thus, a simple viscosity increase would actually shift the Reynolds number to values much lower than the critical value required for vortex shedding!

### 4.3. *Implications for filament inhibition and drag reduction in turbulent flows*

The results of this work suggest three mechanisms through which polymers could inhibit the formation of vorticity filaments in turbulent flows (Bonn *et al.* 1993; Cadot *et al.* 1998). Recall that the process of filament formation is similar to the sequence of instabilities which occur in mixing layers and body wakes (Cadot *et al.* 1995). Specifically, this involves a roll-up instability of an inflectional velocity profile followed by a three-dimensional instability. In the first mechanism of filament inhibition, the polymers act by simply slowing the growth rate of the two-dimensional instability, meaning that fewer filaments form in a given time. In the second mechanism, the polymers act in the nonlinear regime of the instability. The resulting two-dimensional vortices then have a shape or arrangement which does not support strong growth of three-dimensional disturbances. The third mechanism is a stretching inhibition leading to less-concentrated vorticity filaments (cf. § 3.4 and Sureshkumar *et al.* 1997). These mechanisms are not mutually exclusive (e.g. figure 6(*b*) shows a case where the polymers both slow the growth rate and change the two-dimensional vortices), and all probably operate in a turbulent flow. In addition, the study of Yarin (1997) indicates that once the filaments do form, they should be more difficult to break apart.

It is also possible to construct some tentative arguments about drag reduction mechanisms by combining our observations of instability inhibition along with the idea of a turbulent energy cascade. Consider first the case of homogeneous isotropic turbulence, where the energy is injected at a large scale of typical size $L$ and velocity $U$. The energy is then transferred in a very efficient way, through the inertial range of typical sizes $l$ and velocities $u$, to the smallest scale where dissipation occurs. In the case of turbulence which is stationary in time, the power injected into the flow is equal to the power transferred in the inertial range and also equal to the power dissipated. From the Kolmogorov scaling (Frish 1995), an eddy of the inertial range having size $l$ and velocity $u$ transfers to the smaller scales a kinetic energy per unit of mass $u^2$ during the time $l/u$. The power per unit of mass that is transferred through the scale $l$ is then $\epsilon = u^3/l$. Since the turbulence is stationary, the same transferred power occurs at any scale of the inertial range, meaning that the dissipated power and

injected power per unit of mass are also given by $\epsilon$. Assuming that inhibition of the two-dimensional instabilities of inflectional velocity profiles corresponds to a slower rate of production of large-scale inertial eddies of energy per unit mass $U^2$, a time longer than $L/U$ will be required to transfer the same amount of energy if the eddy size remains the same. (It is possible that the eddies resulting from two-dimensional roll-ups may decrease in size, as suggested by the experiments of Riediger 1989 and simulations of Kumar & Homsy 1999.) An immediate consequence is that $\epsilon$ becomes smaller, which implies a reduction of the dissipated power. A second consequence of the stabilization mechanism is that the range of the inertial scales becomes smaller: the large scale remains the same but the dissipation scale $l_\eta \sim \nu^{3/4}/\epsilon^{1/4}$ becomes larger. Small-scale truncation of the inertial range is observed by McComb *et al.* (1977), but only for concentrations larger than 200 w.p.p.m. of PEO. In the scheme we have outlined, dissipation reduction would occur if the polymer significantly affects the rate of production of large-scale inertial structures through which the energy is injected into the turbulent flow. Even though the polymers may experience strong stretching at small scales, this does not preclude their action at large scales. These arguments may also apply to boundary-layer-forced turbulence if there exists some sort of an energy cascade. Support for this idea comes from the fact that drag reduction is not observable in the case of forced turbulence with a fixed rate of production of large scales (Cadot *et al.* 1998), while there is a drastic reduction observable in boundary-layer-forced turbulence (Lumley 1969; Berman 1978) where no rate of production of the large scales is imposed. The intermediate case was investigated by Virk (1970), who showed that in the case of a rough pipe, the roughness inhibits the drag reduction effects. Finally, we note that these arguments do not say anything about how polymers affect velocity fluctuations, an issue that needs to be addressed in a complete drag reduction theory.

We make several other points about the above discussion. First, the idea that inhibition of inflectional instabilities is important in the drag reduction process has also been suggested by Landahl & Bark (1975). They considered the effect of polymers on the stability of an inflectional velocity profile. By modelling the stretched polymers using a constitutive model for fibre suspensions, they found that two-dimensional instabilities could indeed be stabilized. Second, inhibition of filament formation may not necessarily be connected with drag reduction. In the experiments of Cadot *et al.* (1998), no change in the number of filaments was observed during the homogeneous regime of drag reduction. This indicates that filament formation is a rare event, and that the observed filament breakdown probably does not make a large contribution to the average energy dissipation. Third, since the instability inhibition we have observed occurs with semi-dilute polymer solutions, our ideas are more relevant to heterogeneous drag reduction, where a semi-dilute polymer solution is injected into the flow. They may also be relevant to homogeneous drag reduction by dilute solutions if the solution used actually contains some macromolecular aggregates (Hinch & Elata 1979).

## 5. Conclusion

Experiments in which polymer solutions are injected into a cylinder wake provide a way to study viscoelastic effects on two- and three-dimensional shear instabilities. We find that viscoelasticity appears to delay the development of the two-dimensional instability and shifts it to longer wavelengths. In addition, the three-dimensional A mode tends to be damped, and this is correlated with changes in the aspect

ratio of the two-dimensional wake. In the rare cases that the A mode does appear, its wavelength is governed by the two-dimensional wavelength and the streamwise stretching appears to be inhibited. The stabilizing effect of viscoelasticity on these two- and three-dimensional shear instabilities suggests mechanisms for the way polymers inhibit formation of vorticity filaments and reduce drag in turbulent flows.

We thank Y. Couder and S. Douady for their interest and for fruitful discussions throughout the experiments. We are grateful to O. J. Crumeyrolle and M. Grisel for performing the rheological measurements on our solutions and to the laboratory (UMR CNRS 6522) Polymères, Biopolymères et Membranes of Rouen (France) for providing the rheometer. S. Kumar thanks the National Science Foundation (NSF-NATO Postdoctoral Fellowship) and Ecole Normale Supérieure for their financial support.

## REFERENCES

Azaiez, J. & Homsy, G. M. 1994 Linear stability of free shear flow of viscoelastic liquids. *J. Fluid Mech.* **268**, 37.

Berger, E. & Wille, R. 1972 Periodic flow phenomena. *Ann. Rev. Fluid Mech.* **4**, 313.

Berman, N. S. 1978 Drag reduction by polymers. *Ann. Rev. Fluid Mech.* **10**, 47.

Bernal, L. P. & Roshko, A. 1986 Streamwise vortex structure in plane mixing layers. *J. Fluid Mech.* **170**, 499.

Bewersdorff, H. W., Gyr, A., Hoyer, K. & Tsinober, A. 1993 An investigation of possible mechanisms of heterogeneous drag reduction in pipe and channel flows. *Rheol. Acta* **32**, 140.

Bird, R. B., Armstrong, R. C. & Hassager, O. 1987*a* *Dynamics of Polymeric Liquids, Volume 1: Fluid Mechanics*. Wiley.

Bird, R. B., Curtiss, C. F., Armstrong, R. C. & Hassager, O. 1987*b* *Dynamics of Polymeric Liquids, Volume 2: Kinetic Theory*. Wiley.

Bonn, D., Couder, Y., Dam, P. H. J. van & Douady, S. 1993 From small scales to large scales in three dimensional turbulence. *Phys. Rev.* E **47**, R28.

Brede, M., Eckelmann, H. & Rockwell, D. 1996 On secondary vortices in the cylinder wake. *Phys. Fluids* **8**, 2117.

Cadot, O., Bonn, D. & Douady, S. 1998 Turbulent drag reduction in a closed flow system: boundary layer vs. bulk effects. *Phys. Fluids* **10**, 426.

Cadot, O., Douady, S. & Couder, Y. 1995 Characterization of the low-pressure filaments in a three-dimensional turbulent shear flow. *Phys. Fluids* **7**, 630.

Cadot, O. & Lebey, M. 1999 Shear instability inhibition in a cylinder wake by local injection of a viscoelastic fluid. *Phys. Fluids* **11**, 494.

Delvaux, V. & Crochet, M. J. 1990 Numerical prediction of anomalous transport properties in viscoelastic flow. *J. Non-Newtonian Fluid Mech.* **37**, 297.

Doi, M. & Edwards, S. F. 1986 *The Theory of Polymer Dynamics*. Oxford University Press.

Douady, S., Couder, Y. & Brachet, M.-E. 1991 Direct observation of the intermittency of intense vorticity filaments in turbulence. *Phys. Rev. Lett.* **67**, 982.

Frisch, U. 1995 *Turbulence: The Legacy of A. N. Kolmogorov*. Cambridge University Press.

Georgelos, P. N. & Torkelson, J. M. 1988 The role of solution structure in apparent thickening behaviour of dilute PEO/water systems. *J. Non-Newtonian Fluid Mech.* **27**, 191.

Graessley, W. W. 1980 Polymer chain dimensions and the dependence of viscoelastic properties on concentration, molecular weight, and solvent power. *Polymer* **21**, 258.

Hibberd, M., Kwade, M. & Scharf, R. 1982 Influence of drag reducing additives on the structure of turbulence in a mixing layer. *Rheol. Acta* **21**, 582.

Hinch, E. J. 1977 Mechanical models of dilute polymer solutions in strong flows. *Phys. Fluids* **20**, S22.

Hinch, E. J. & Elata, C. 1979 Heterogeneity of dilute polymer solutions. *J. Non-Newtonian Fluid Mech.* **5**, 411.

James, D. F. & Acosta, A. J. 1970 The laminar flow of dilute polymer solutions around circular cylinders. *J. Fluid Mech.* **42**, 269.

Jimenez, J. & Wray, A. A. 1998 On the characteristics of vortex filaments in isotropic turbulence. *J. Fluid Mech.* **373**, 255.

Joseph, D. D. 1990 *Fluid Dynamics of Viscoelastic Liquids*. Springer.

Kalashnikov, V. N. & Kudin, A. M. 1970 Karman vortices in the flow of drag-reducing polymer solutions. *Nature* **225**, 445.

Kármán, T. von 1911 Uber der mechanismus des widerstandes, den ein bewegter koeper in einer fluessigkeit erfaehrt. *Gottinger Nachrichten Math-Phys*, KI 547.

Kida, S. & Miura, H. 1998 Identification and analysis of vortical structures. *Eur. J. Mech.* B/*Fluids* **17**, 471.

Kim, B. K. & Telionis, D. P. 1989 The effect of polymer additives on laminar separation. *Phys. Fluids* A **1**, 267.

Konuita, A., Adler, P. M. & Piau, J.-M. 1980 Flow of dilute polymer solutions around circular cylinders. *J. Non-Newtonian Fluid Mech.* **7**, 101.

Kumar, S. & Homsy, G. M. 1999 Direct numerical simulation of hydrodynamic instabilities in two- and three-dimensional viscoelastic free shear layers. *J. Non-Newtonian Fluid Mech.* **83**, 251.

Landahl, M. T. & Bark, F. H. 1975 Application of a two-scale boundary layer turbulence model to drag reduction. In *Colloques Internationaux du CNRS, Polymres et Lubrification*, **233**, 249.

Leweke, T. & Williamson, C. H. K. 1998*a* Cooperative elliptic instability of a vortex pair. *J. Fluid Mech.* **360**, 85.

Leweke, T. & Williamson, C. H. K. 1998*b* Three-dimensional instabilities in wake transition. *Eur. J. Mech.* B/*Fluids* **17**, 571.

Lin, S. J. & Corcos, G. M. 1984 The mixing layer: deterministic models of a turbulent flow. Part 3. The effect of plane strain on the dynamics of streamwise vortices. *J. Fluid Mech.* **140**, 139.

Lumley, J. L. 1969 Drag reduction by additives. *Ann. Rev. Fluid Mech.* **1**, 366.

McComb, W. D., Allan, J. & Greated, C. A. 1977 Effect of polymer additives on the small-scale structure of grid generated turbulence. *Phys. Fluids* **20**, 873.

Mizushina, T. & Usui, H. 1975 Transport phenomena of viscoelastic fluid in cross flow around a circular cylinder. *J. Chem. Engng Japan* **8**, 393.

Neu, J. C. 1984 The dynamics of stretched vortices. *J. Fluid Mech.* **143**, 253.

Passot, T., Politano, H., Sulem, P. L., Angilella, J. R. & Meneguzzi, M. 1995 Instability of strained vortex layers and vortex tube formation in homogeneous turbulence. *J. Fluid Mech.* **282**, 313.

Riediger, S. 1989 Influence of drag reducing additives on a plane mixing layer. In *Drag Reduction in Fluid Flows* (ed. R. H. J. Sellin & R. T. Moses). Ellis Horwood.

Sarpkaya, T., Rainey, P. G. & Kell, R. E. 1973 Flow of dilute polymer solutions about circular cylinders. *J. Fluid Mech.* **57**, 177.

Shiang, A. H., Lin, J. C., Oztekin, A. & Rockwell, D. 1997 Viscoelastic flow around a confined circular cylinder: measurements using high-image-density particle image velocimetry. *J. Non-Newtonian Fluid Mech.* **73**, 29.

Siggia, E. D. 1981 Numerical study of small-scale intermittency in three-dimensional turbulence. *J. Fluid Mech.* **107**, 375.

Sreenivasan, K. R. & Antonia, R. A. 1997 The phenomenology of small-scale turbulence. *Ann. Rev. Fluid Mech.* **29**, 435.

Sureshkumar, R., Beris, A. N. & Handler, R. A. 1997 Direct numerical simulation of the turbulent channel flow of a polymer solution. *Phys. Fluids* **9**, 743.

Toms, B. A. 1948 Some observations on the flow of linear polymer solutions through straight tubes at large Reynolds number. In *Proc. First Intl Rheological Congress*. North Holland.

Tong, P., Goldburg, W. I. & Huang, J. S. 1992 Measured effects of polymer additives on the turbulent-velocity fluctuations at various length scales. *Phys. Rev.* A **45**, 7231.

Usui, H., Shibata, T. & Sano, Y. 1980 Karman vortex behind a circular cylinder in dilute polymer solutions. *J. Chem. Engng Japan* **13**, 77.

Villermaux, E., Sixou, B. & Gagne, Y. 1995 Intense vortical structures in grid-generated turbulence. *Phys. Fluids* **7**, 2008.

Virk, P. S. 1970 Drag reduction in rough pipes. *J. Fluid Mech.* **45**, 225.

Vissman, K. & Bewersdorff, H. K. 1997 The influence of pre-shearing on the elongational behavior of dilute polymer and surfactant solutions. *J. Non-Newtonian Fluid Mech.* **34**, 289.

Vlassopoulos, D. & Schowalter, W. R. 1994 Steady properties and characterization of dilute drag-reducing polymer solutions. *J. Rheol.* **38**, 1427.

Vleegaar, J. & Tels, M. 1973 Drag reduction by polymer threads. *Chem. Engng Sci.* **28**, 965.

Williamson, C. H. K. 1989 Oblique and parallel modes of vortex shedding in the wake of a circular cylinder at low Reynolds number. *J. Fluid Mech.* **206**, 579.

Williamson, C. H. K. 1996*a* Vortex dynamics in the cylinder wake. *Ann. Rev. Fluid Mech.* **28**, 477.

Williamson, C. H. K. 1996*b* Three-dimensional wake transition. *J. Fluid Mech.* **328**, 345.

Yarin, A. L. 1997 On the mechanism of turbulent drag reduction in dilute polymer solutions: dynamics of vortex filaments. *J. Non-Newtonian Fluid Mech.* **69**, 137.

Zang, H.-Q., Fey, U., Noack, B. R., Konig, M. & Eckelmann, H. 1995 On the transition of the cylinder wake. *Phys. Fluids* **7**, 779.